PROGRESS REPORT: Since 09/2024, progress has been made on both aims without research plan changes.

Aim 1: To conduct ST on tissue from individuals with EDD and matched biological and healthy controls. In our original research plan, we proposed recruiting and obtaining biopsies for spatial transcriptomics from 60 individuals with epidermal differentiation disorders (EDD, a.k.a. the "ichthyoses"), as well as 16 healthy controls and 8 individuals with inflammatory skin diseases (psoriasis, atopic dermatitis) for biological comparison. In preparation for this application, at the June, 2024 FIRST meeting we had obtained 20 samples from individuals with EDD to be used for spatial transcriptomics. We proposed to focus on more frequent genotypes and cardinal biological pathways driving EDD pathogenesis. These are *TGM1* (cornified envelope), *KRT1*/10 (structural proteins), *NIPAL4*/ALOX12B/ALOXE3 (lipid biosynthesis), *ABCA12* (lipid transport), *GJB2* (intercellular communication), *SPINK5* (protease/desquamation), *FLG* (barrier, severity modifier), and *STS* (lipid metabolism).

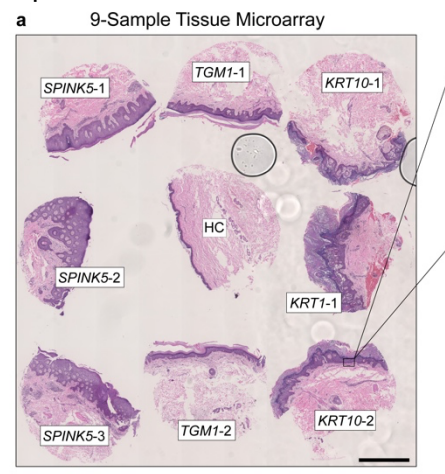
During the first 10 months of our funded period (09/2024 – 06/2025), we succeeded in recruiting and obtaining biopsies from an additional 50 individuals with EDD (total 70 biopsies), 13 healthy controls, and 8 inflammatory skin disease samples. This exceeded our recruitment goal of 20 individuals with EDD in Year 1, largely due to an overwhelming interest in contributing to research at the FIRST 2024 family conference.

The overall status of our study, broken down by genotype, is shown below:

Genotype-Phenotype	Number of Individuals			
	Recruited with Biopsy	Sequenced and Analyzed	Sequencing in Progress	Queued for Se- quencing
TGM1-lamellar phenotype	9	4	5	
TGM1-erythrodermic phenotype	5		5	
KRT10-epidermolytic ichthyosis	7	4	3	
KRT1-epidermolytic ichthyosis	2	2		
KRT10-ichthyosis with confetti	2	2		
ABCA12-recessive ichthyosis	3		3	
ALOX12B-recessive ichthyosis	1		1	
ALOXE3-recessive ichthyosis	1		1	
NIPAL4-recessive ichthyosis	1		1	
PNPLA1-recessive ichthyosis	3	1	2	
SPINK5-Netherton syndrome	3	3		
GJB2-keratitis ichthyosis deafness syndrome	2	1	1	
FLG-ichthyosis vulgaris	1		1	
STS-X linked ichthyosis	1		1	
Other (SLURP1, EMP2, DSP, CARD14, KLK11, KDSR, ASPRV1, GJA1, LOR, NSDHL, CYP4F22, SNAP29, CTSC)	29	15		14
Total Ichthyosis	70	32	24	14
Healthy Controls	13	5	3	5
Inflammatory skin diseases (psoriasis, atopic dermatitis)	8		8	
Total Cohort	91	37	35	19

We made two key technical advances during Year 1, which will enable us to perform ST profiling with the throughput and specificity necessary to obtain statistically rigorous results (**Fig. 1**). First, we improved our tissue microarray (TMA) design to accommodate 9 samples per spatial transcriptomic (ST) capture area rather than 5 samples, as we originally proposed. This affords cost savings, will permit us to sequence more samples, and will help us to obtain more robust results, given phenotypic variability within genotypes.

b 2µm resolution whole-transcriptome profiling



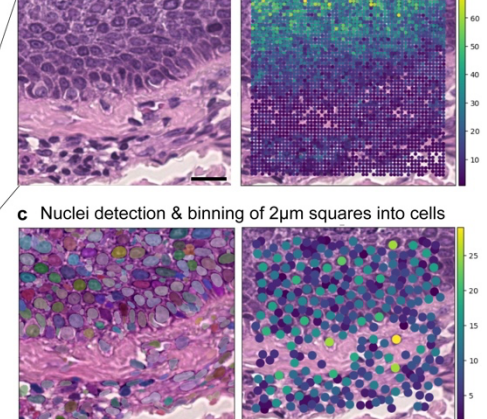


Figure 1: Technical approach for analysis of ST data. (a) Nine samples are arranged into a TMA and profiled on the same capture area of a Visium HD slide. Scale bar denotes 1mm. (b) Inset shows high-resolution capture of the dermal-epidermal junction of epidermolytic ichthyosis sample *KRT10-2* illustrating 2μm capture spots. The heat map on the right shows the number of transcripts in each 2μm capture spot overlaid on the tissue image. Scale bar denotes 20 μm. (c) Nuclei detected in the H&E image (assigned random colors) with *bin2cell*. The heat map on the right shows the number of 2μm capture spot spots binned into each detected cell. HC, healthy control.

Second, we optimized the use of the deep-learning based cell detection algorithm *bin2cell*¹ for cell detection in skin sections profiled with Visium High-Definition (HD). Utilizing this approach allows us to bin the expression from 2 x 2 µm capture spots into individual cells based on nuclei detected in the hematoxylin and eosin-stained image. Performing downstream analysis on a matrix of cells x genes allows us to uncover spatially-resolved cell type-specific molecular programs, significantly improving the specificity of our analysis over approaches which do not perform cell segmentation.¹

Aim 2: To identify shared and distinct molecular mechanisms of EDD across different genotypes. In addition to advances in the technical approach for ST experiments, we have made significant progress in our development of analytical approaches to extract meaningful biological insight from ST data. We utilized ST to study two novel genetic causes of progressive symmetric erythrokeratoderma

(PSEK), a phenotype within the EDD spectrum, described below.

SLURP1 A22 mutations cause autosomal dominant PPK and PSEK.

In our EDD cohort, three unrelated kindreds (P342, P377, P446) presented with distinct phenotypes of palmoplantar keratoderma (PPK), with or without well-demarcated pink-red scaly plaques (PSEK). All were found to have *SLURP1* heterozygous variants at the same amino acid position within the signal peptide sequence (p.A22D and A22V). However, we observed a distinct phenotype for each genotype, with the p.A22V variant associated with isolated, severe PPK, and the p.A22D variant with thick PPK and PSEK (**Fig. 2a**). Histopathology showed hyperkeratosis, acanthosis, and mild lymphocytic infiltration in the superficial dermis (**Fig. 2b**). Differentiation markers, including KRT14 and involucrin, had expanded expression compared to healthy control, and the absolute percentage of basal Ki67+ cells, indicative of proliferation, was higher in affected skin (32.5% in P377 and 36.9% in P342) compared to healthy controls (5.7%).

SLURP1 encodes a secreted protein with a 22-amino acid N-terminal signal peptide (SP) required for ER translocation and cleavage by membrane-bound type I signal peptidases.^{2,3} A22 is the terminal residue of the SP, so we examined whether the A22D and A22V variants affect SLURP1 processing or secretion. Under basal conditions, SLURP1 expression

Figure 2: Dominant SLURP1 mutations cause PPK and PSEK. (a) Affected individuals PPK377-1 (A22D) and PPK446-2 (A22D) exhibited diffuse PPK and well-demarcated scalp, pink-red, thickened plaques with fine scales on the trunk and extremities. PPK342-1 (A22V) showed diffuse transgrediens PPK with tapering of the digits. (b) Histopathological analysis of a plaques on the torso showed hyperkeratosis, acanthosis and mild lymphocytic infiltration in the

superficial dermis. Scale bar = 100 μm.

b

and secretion in patient-derived keratinocytes were comparable to those in healthy controls. However, upon calcium-induced differentiation, keratinocytes carrying the A22D or A22V variants exhibited increased intracellular and secreted SLURP1 protein levels, with no alteration in molecular weight, suggesting enhanced SLURP1 expression and secretion rather than impaired cleavage. Immunofluorescence staining confirmed increased SLURP1 expression in patient skin (**Fig. 3a, b**).

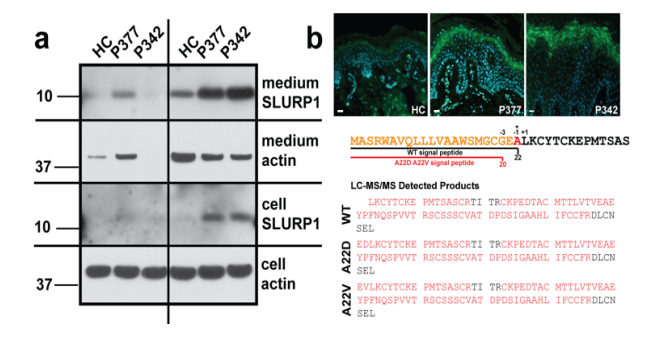


Figure 3: A22V/D SLURP1 mutations increase secretion. (a) SLURP1 expression was elevated in differentiated keratinocytes and media from individuals with A22D (PPK377) and A22V (PPK342) variants compared to healthy controls (HC). No significant expression was seen under basal conditions. (a) Western blot showed increased SLURP1 in differentiated cells and media. (b) Immunofluorescence revealed expanded SLURP1 in the upper spinous and granular layers of patient epidermis. LC-MS/MS confirmed altered cleavage sites in both variants, with distinct peptides from WT. Scale bars = 20 μm.

SignalP6.0 analysis predicted a two-amino acid upstream shift in the SP cleavage site for both A22D and A22V variants. LC-MS/MS analysis of secreted mutant SLURP1-FLAG protein from pLVX-transduced SCC25 cells confirmed the presence of two additional N-terminal amino acids, validating the altered cleavage site (**Fig. 3b**).

High-resolution spatial transcriptomic profiling of SLURP1-PSEK skin revealed upregulation of genes involved in terminal differentiation (e.g., *SPRR1B*, *SPRR2D*, *SPRR2E*, *SPRR2G*) and innate immune response (e.g., *S100A8*, *S100A9*, *IL36G*). Suprabasal keratinocytes displayed a damage-associated transcriptional signature with elevated *KRT6A/B* and *KRT16*, and reduced *KRT1* and *KRT10*.^{4–8} Pathway enrichment analysis identified NF-κB signaling as the top dysregulated pathway. Keratinocyte-specific NF-κB target genes were markedly upregulated in the upper spinous layer, suggesting that increased SLURP1 expression and secretion may activate NF-κB signaling downstream of α7-nicotinic

acetylcholine receptor (α 7-nAChR) engagement. ^{9,10} There are multiple NF- κ B inhibitors that have been investigated in cancer and inflammation that could be candidates for treating SLURP1-PSEK, including sulfasalazine, triptolide, and small molecule inhibitors. We are testing these compounds in vitro to assess capacity to normal-

ize gene expression.

EMP2 L4P mutation causes PPK and PSEK. We identified two unrelated individuals (PSEK-623 and PSEK-1574) carrying an identical heterozygous, *de novo* missense pathogenic variant in exon 1 of *EMP2* (p.L4P). Both probands exhibited thick, red, scaly periorificial and intertriginous plaques, along with painful palmoplantar keratoderma exacerbated by ambulation. Histopathology revealed acanthosis, hyperkeratosis, and parakeratosis. (**Fig. 4**)

To investigate disease pathobiology, we performed high-resolution spatial transcriptomics on affected skin from PSEK-1574 compared to healthy donor skin. Affected epidermis demonstrated increased expression of transcripts involved in terminal differentiation and desquamation, including *KLK6*, *KLK7*, *KLK8*, *KLK10*, *S100A8*, *S100A9*, and damage-associated keratins *KRT6* and *KRT16*. Multiple growth factor—related transcripts were overexpressed, notably those in the MAPK pathway and the transcription factor *JUNB*. Gene set

PSEK-623

Figure 4: EMP2 mutation causes PSEK. (a) PSEK-623 (13 years) and PSEK-1574 (21 months) show well-demarcated red, scaly plaques in periorificial and flexural areas. PSEK-623 displays thick moccasin-like scaling of the soles, while PSEK-1574 has milder involvement and developed new lesions after gastrostomy-related trauma. (b) Histology shows epidermal and stratum corneum thickening with retained nuclei (black arrow), consistent with hyperproliferation, and sparse lymphocytic and eosinophilic infiltrates. Scale bars, 50 μm.

enrichment analysis revealed the top overlapping pathways involved epidermal growth factor receptor (EGFR) family kinases. In control skin, EGFR activation decreased in suprabasal layers as differentiation progressed, consistent with prior reports.¹¹ In contrast, the EGFR activation score was significantly elevated across all epidermal layers in PSEK-1574, with a further increase in suprabasal spinous layers. (**Fig. 5**)

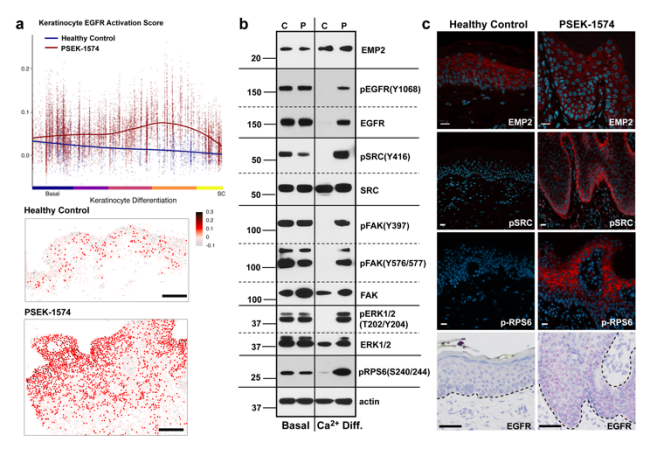


Figure 5: Ectopic EGFR activation in *EMP2*-PSEK (a) Via ST, EGFR activation scores were significantly higher in PSEK-1574 epidermis compared to healthy control (p < 0.0001, a lower panels), and expression increases ectopically during differentiation (a, upper). (b) Immunoblotting confirmed this finding and showed increased total EGFR and phosphorylated Src, FAK, ERK, and RPS6 in differentiated PSEK-1574 keratinocytes, with no change in EMP2 levels. C, healthy control; P, PSEK-1574. (c) Immunofluorescence showed cytoplasmic EMP2 in basal layers and membrane localization in suprabasal cells in both PSEK and control skin. Phospho-RPS6 and pSRC were elevated in affected but absent in control epidermis. Affected skin (PSEK-1574) showed increased EGFR expression in the epidermis compared to healthy control skin by RNA in situ hybridization. Red dots indicate EGFR transcripts, counterstained with hematoxylin. Scale bars, 20 μm.

Immunoblotting of differentiated keratinocytes from PSEK-1574 confirmed ST findings and revealed increased total EGFR and marked elevation of phosphorylated Src (Y416), FAK (Y397, Y576/577), ERK, and RPS6 (S240/244) compared to healthy controls. Immunostaining confirmed increased pSrc and pRPS6 levels in affected skin. EGFR transcript levels were also elevated in PSEK epidermis, as demonstrated by RNA in situ hybridization.

To identify potential mediators of EMP2 function, we conducted miniTurbo proximity labeling¹² in keratinocytes expressing either wild-type or L4P EMP2-miniTurbo fusion pro-

teins. After stringent filtering, 361 high-confidence EMP2 interactors were identified. Pathway analysis revealed enrichment in cell-cell adhesion and transmembrane receptor tyrosine kinase signaling. Analysis using the DGldb Drug Targets 2024 database showed strong enrichment for tyrosine kinase-related proteins and ephrin re-



Figure 6: Erlotinib treatment improves EMP2-PESK. One year of treatment with 75 mg of erlotinib daily in PSEK-623 led to a significant response, with complete elimination of hyperkeratotic plaques in the armpit and trunk, although hypopigmentation remained.

after erlotinib

ceptors, with the top 10 enriched drug targets being tyrosine kinase inhibitors. Prior data suggested that treatment with erlotinib, an EGFR inhibitor, is effective and well-tolerated in pachyonychia congenita. Therefore, proband PSEK-623 was treated with the EGFR inhibitor erlotinib (75 mg/day). After one month, hyperkeratotic plaques on the armpits and trunk resolved, leaving residual hypopigmentation (**Fig. 6**).

Advances in ST analysis. We have made significant progress in developing the computational framework for integrative analysis of ST data across the spectrum of EDD genotypes. We developed a data integration approach which makes use of the *Harmony*¹³ algorithm to generate a shared gene expression embedding across all samples (**Fig. 7**). Using an integrated dataset of our first 37 samples, we identified 10 conserved cell types present in all samples and a rich diversity of gene expression programs within keratinocytes of the interfollicular epidermis. This cell type identification allows us to assign altered gene expression programs to specific cell types in the skin, such as suprabasal keratinocytes or T cells, which represents a significant advance on prior transcriptomic studies of ichthyosis, which utilized bulk RNA sequencing.

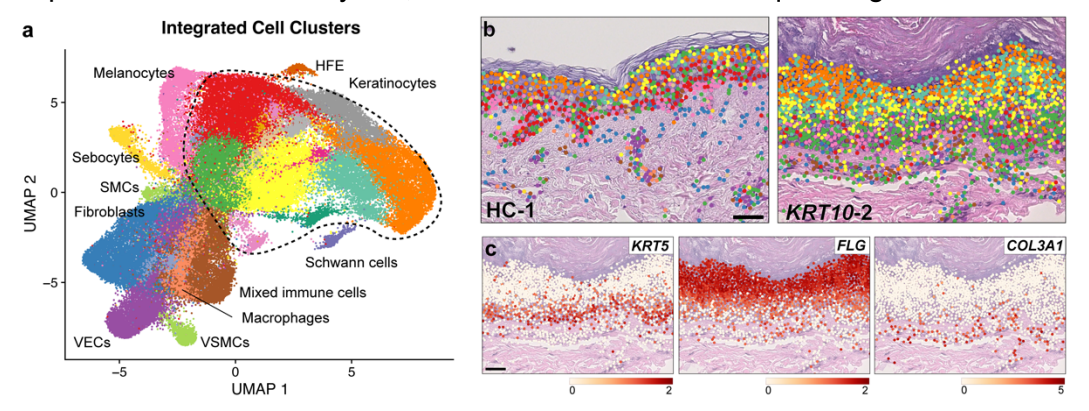


Figure 7: Identification of conserved cell types in skin from ST data. (a) Data from all 37 samples was integrated using *Harmony* and 2,000 cells from each sample are shown in the UMAP plot on the left. Different colors indicate the result of unsupervised clustering based on gene expression data. (b) Cell clusters are overlaid on the H&E image for one healthy control sample and one *KRT10* epidermolytic ichthyosis sample. (c) Normalized expression levels of key cell-type defining genes overlaid on the H&E image of sample *KRT10-2*: *KRT5*, basal keratinocyte marker, *FLG*, suprabasal keratinocyte marker. *COL3A1*, fibroblast marker. UMAP, uniform manifold approximation and projection. HFE, hair follicle epidermis, VEC, vascular endothelial cell. VSMC, vascular smooth

From our integrated dataset, we have optimized the use of non-negative matrix factorization (NMF)¹⁴ to compute unbiased modules of genes which are co-expressed across the dataset. We performed NMF on the entire dataset and defined 20 gene modules. We then computed the enrichment of each gene module in each sample, with genotypes for which we have more than one sample. This analysis revealed pathways which are broadly shared

across EDD genotypes: the NMF module 14 was increased above healthy control levels in 14 out of 15 affected individuals. (**Fig. 8**) Top-contributing genes to module 14 include *S100A2*, which has been shown to be associated with keratinocyte damage, ¹⁵ *GJB2* which is associated with wound healing and epidermal hyperproliferation, ¹⁶ and multiple histone transcripts which may indicate increased cell division and epidermal hyperproliferation. Notably, this gene module is largely localized to basal layer keratinocytes, which suggests that this

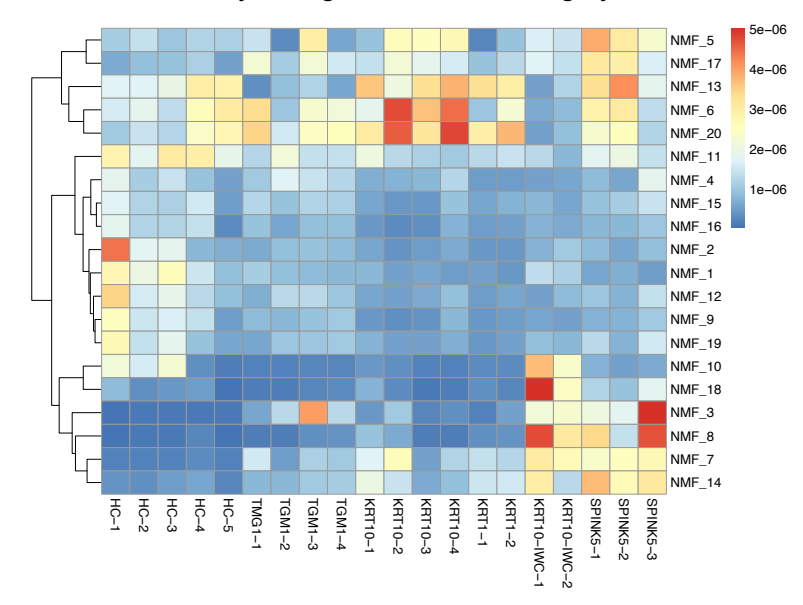


Figure. 8: Unbiased identification of shared and distinct molecular programs across EDD. Non-negative matrix factorization (NMF) gene modules were computed across the entire dataset. The heatmap shows the enrichment of each NMF module for each sample for genotypes in which we have more than one individual sequenced. NMF modules are clustered according to their enrichment across the samples. HC, healthy control.

gene signature may partially explain epidermal hyperproliferation shared across most EDD subtypes

This analysis also suggests molecular alterations that are specific to certain EDD subtypes. For example, NMF module 8, which contained transcripts for keratins associated with keratinocyte cell stress such as KRT6A/B/C and KRT16 was increased in samples from individuals with ichthyosis with confetti due to KRT10 variants and Netherton syndrome due to SPINK5 variants. This suggests that a cell stress signature is shared between these two diseases and may explain the prominent erythema that these two diseases share. The NMF modules 6 and 20 were increased in epidermolytic ichthyosis (EI) samples due to KRT1 or KRT10 variants. These modules contained transcripts of structural proteins important for terminal differentiation, such as FLG and LOR, which have been observed to be increased in El skin.17

In order to better understand the immunopathogenesis of different types of EDD, we also collected noninvasive skin swabs from individuals enrolled in our ST study, using a detergent-based immune profiling system¹⁸ to collect proteins from skin. We performed multiplex proteomic analysis of the skin protein samples using other funding and found that certain individuals with EDD

share a broad immune activation with up-regulation of chemokines and cytokines related to the Th17 and Th1 pathways (**Fig. 9**). We will continue to collect this non-invasive protein samples on individuals enrolled in our study, in order to correlate gene signatures discovered in ST data with changes in immune-related proteins.

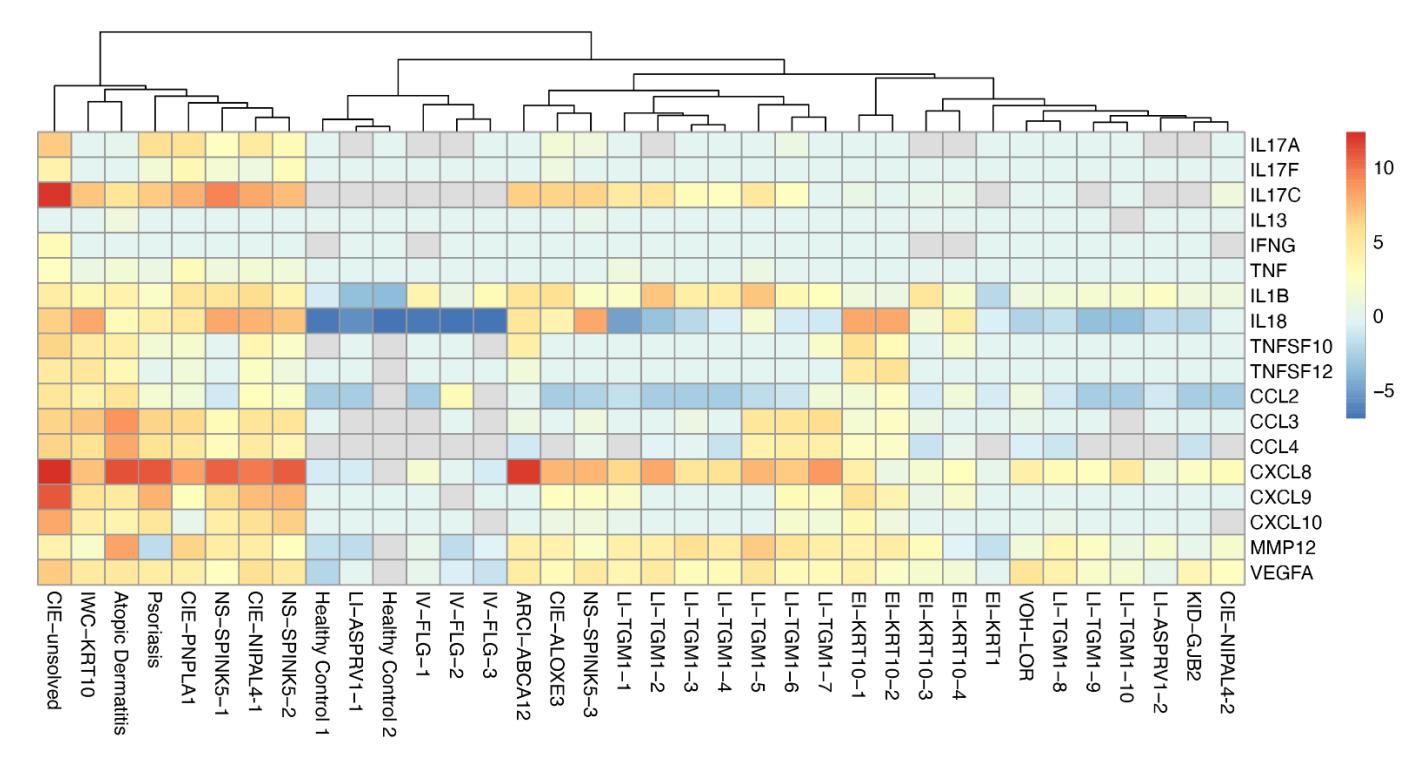


Fig. 9: Cytokine profiling from non-invasive skin swabs. Non-invasive detergent-based epidermal sampling was performed on 32 individuals with EDD and 3 healthy controls, and multiplex cytokine measurements (Olink Target 48 Cytokine) were compared to samples from psoriasis and atopic dermatitis from Murphy *et al.* Color bar indicates expression of each immune marker, normalized by row. CIE, congenital ichthyosiform erythroderma. IWC, ichthyosis with confetti, NS, Netherton syndrome. IV, ichthyosis vulgaris. ARCI, autosomal recessive congenital ichthyosis. LI, lamellar ichthyosis. EI, epidermolytic ichthyosis. VOH, Vohwinkel Syndrome. KID, keratitis ichthyosis deafness syndrome.

<u>Summary:</u> The single-cell spatial transcriptomic atlas of EDD supported by FIRST is already advancing our understanding of the molecular underpinnings of scale and erythema in EDD patients and will serve as a valuable resource for basic and translational research, including identification of targets for therapeutic intervention. In Year 1, we have made key technical advances in the experimental methodology for performing single-cell resolution spatial transcriptomics across a wide number of samples from individuals with EDD. We have also advanced our analytical approaches for deriving biological insight from ST datasets, with two strong examples where we have used ST to inform therapeutic approaches in monogenic ichthyoses. We have supplemented our ST dataset by performing complementary proteomic analysis of noninvasive skin swabs, which will strengthen our findings on immune signatures in EDD. Our efforts in the first 10 months of the funded period lay the groundwork for continued development of this multi-omic effort to understand dysregulated pathways in EDD and develop new therapeutic approaches.

References

- Polański K, Bartolomé-Casado R, Sarropoulos I, Xu C, England N, Jahnsen FL, Teichmann SA, Yayon N. Bin2cell reconstructs cells from high resolution Visium HD data. Bioinformatics. 2024 Sep 1;40(9):btae546.
- Shulepko MA, Bychkov ML, Shenkarev ZO, Kulbatskii DS, Makhonin AM, Paramonov AS, Chugunov AO, Kirpichnikov MP, Lyukmanova EN. Biochemical Basis of Skin Disease Mal de Meleda: SLURP-1 Mutants Differently Affect Keratinocyte Proliferation and Apoptosis. J Invest Dermatol. 2021 Sep;141(9):2229– 2237. PMID: 33741389
- 3. Choo KH, Ranganathan S. Flanking signal and mature peptide residues influence signal peptide cleavage. BMC Bioinformatics. 2008 Dec 12;9(12):S15.
- 4. Thorey IS, Roth J, Regenbogen J, Halle JP, Bittner M, Vogl T, Kaesler S, Bugnon P, Reitmaier B, Durka S, Graf A, Wöckner M, Rieger N, Konstantinow A, Wolf E, Goppelt A, Werner S. The Ca2+-binding Proteins S100A8 and S100A9 Are Encoded by Novel Injury-regulated Genes*. Journal of Biological Chemistry. 2001 Sep 21;276(38):35818–35825.
- 5. Vogl T, Tenbrock K, Ludwig S, Leukert N, Ehrhardt C, van Zoelen MAD, Nacken W, Foell D, van der Poll T, Sorg C, Roth J. Mrp8 and Mrp14 are endogenous activators of Toll-like receptor 4, promoting lethal, endotoxin-induced shock. Nat Med. Nature Publishing Group; 2007 Sep;13(9):1042–1049.
- 6. Mansbridge JN, Knapp AM. Changes in keratinocyte maturation during wound healing. J Invest Dermatol. 1987 Sep;89(3):253–263. PMID: 2442269
- 7. Paladini RD, Takahashi K, Bravo NS, Coulombe PA. Onset of re-epithelialization after skin injury correlates with a reorganization of keratin filaments in wound edge keratinocytes: defining a potential role for keratin 16. J Cell Biol. 1996 Feb;132(3):381–397. PMCID: PMC2120730
- McGowan K, Coulombe PA. The wound repair-associated keratins 6, 16, and 17. Insights into the role of intermediate filaments in specifying keratinocyte cytoarchitecture. Subcell Biochem. 1998;31:173–204. PMID: 9932493
- 9. Hinata K, Gervin AM, Jennifer Zhang Y, Khavari PA. Divergent gene regulation and growth effects by NF-kappa B in epithelial and mesenchymal cells of human skin. Oncogene. 2003 Apr 3;22(13):1955–1964. PMID: 12673201
- Swamynathan S, Campbell G, Sohnen P, Kaur S, St. Leger AJ, Swamynathan SK. The Secreted Ly6/uPAR-Related Protein 1 (Slurp1) Modulates Corneal Angiogenic Inflammation Via NF-κB Signaling. Investigative Ophthalmology & Visual Science. 2024 Jan 22;65(1):37.
- 11. Getsios S, Simpson CL, Kojima S ichiro, Harmon R, Sheu LJ, Dusek RL, Cornwell M, Green KJ. Desmoglein 1–dependent suppression of EGFR signaling promotes epidermal differentiation and morphogenesis. Journal of Cell Biology. 2009 Jun 22;185(7):1243–1258.
- Branon TC, Bosch JA, Sanchez AD, Udeshi ND, Svinkina T, Carr SA, Feldman JL, Perrimon N, Ting AY. Efficient proximity labeling in living cells and organisms with TurbolD. Nat Biotechnol. 2018 Oct;36(9):880–887. PMCID: PMC6126969
- 13. Korsunsky I, Millard N, Fan J, Slowikowski K, Zhang F, Wei K, Baglaenko Y, Brenner M, Loh PR, Raychaudhuri S. Fast, sensitive and accurate integration of single-cell data with Harmony. Nat Methods. 2019 Dec;16(12):1289–1296. PMCID: PMC6884693
- 14. Lin X, Boutros PC. Optimization and expansion of non-negative matrix factorization. BMC Bioinformatics. 2020 Jan 6;21:7. PMCID: PMC6945623

- 15. Yoshioka M, Sawada Y, Saito-Sasaki N, Yoshioka H, Hama K, Omoto D, Ohmori S, Okada E, Nakamura M. High S100A2 expression in keratinocytes in patients with drug eruption. Sci Rep. Nature Publishing Group; 2021 Mar 9;11(1):5493.
- Djalilian AR, McGaughey D, Patel S, Seo EY, Yang C, Cheng J, Tomic M, Sinha S, Ishida-Yamamoto A, Segre JA. Connexin 26 regulates epidermal barrier and wound remodeling and promotes psoriasiform response. J Clin Invest. 2006 May;116(5):1243–1253. PMCID: PMC1440704
- 17. Ishida-Yamamoto A, Eady RA, Underwood RA, Dale BA, Holbrook KA. Filaggrin expression in epidermolytic ichthyosis (epidermolytic hyperkeratosis). Br J Dermatol. 1994 Dec;131(6):767–779. PMID: 7531997
- Murphy MJ, Chen G, Edemobi P, Junejo MH, Wride AM, Spaulding SL, Wang Y, Cohen JM, Damsky W. Non-invasive epidermal proteome assessment-based diagnosis and molecular subclassification of psoriasis and eczematous dermatitis [Internet]. medRxiv; 2024 [cited 2025 Jul 9]. p. 2024.09.24.24314282. Available from: https://www.medrxiv.org/content/10.1101/2024.09.24.24314282v1